Int J Adv Manuf Technol (2016) 84:843–850
DOI 10.1007/s00170-015-7692-z

ORIGINAL ARTICLE

A novel analytical approach to predict rolling force in hot strip finish rolling based on cosine velocity field and equal area criterion

Dian-Hua Zhang[1] · **Yuan-Ming Liu**[1] · **Jie Sun**[1] · **De-Wen Zhao**[1]

Received: 14 May 2015 / Accepted: 3 August 2015 / Published online: 4 September 2015

Abstract In hot strip rolling process, rolling schedule setup, geometrical accuracy (thickness and profile), and even the final product homogeneity of mechanical properties are affected by the automatic control, and the rolling force and torque are the prerequisite in the control process. A new cosine velocity field is firstly proposed in this paper to get the values of the required minimum rolling force and torque. The field and equal area (EA) yield criterion are used to integrate the internal plastic deformation power. Using the co-line vector inner product method, the friction power is analyzed. Finally, the analytical expressions of rolling force, rolling torque, and stress effective factor are obtained. The theoretical predictions of rolling forces are compared with on-line measured ones in a hot strip rolling plant and other researchers' models. Results show that the calculated rolling forces are in fair agreement with the actual measured ones, and the proposed solution is considered to be applicable for solving hot strip finish rolling.

Keywords Cosine velocity field · EA yield criterion · Co-line vector inner product · Analytical solution

1 Introduction

Automatic control system has become significant for the mass manufacturing due to production cost and flexibility, manipulating security and requirement of skilled workers under the increasing global competition in the steel plant circumstance. Accurate prediction of the rolling force and torque is a major issue for obtaining better automation control of production line in hot strip rolling. There have been many researchers developing some approximate methods to predict the rolling force and torque. These can be divided into two groups: numerical solution based on finite element method (FEM) and analytical solution.

Analytical solution is one of the methods to predict the rolling force. Hill [1] proposed a theoretical approach about the stress/strain analysis of processes for mechanical working or forming metals. A kinematically admissible velocity field based on the concept suggested by Hill has been proposed by Oh and Kobayashi [2] to investigate the side spread in flat rolling. An approach for analyzing plane strain rolling is presented by Martins PAF [3] combining upper-bound method and weighted residual method. The dual-stream function velocity field was derived by Sezek et al. [4] to analyze cold and hot plate rolling.

To study complex deformation, FEM is one of the best ways. Kobayashi [5] used FEM to investigate metal forming in flat rolling, and this is an early research work. Mori and Osakada [6] used rigid-plastic FEM to analyze changes of the strip appearance and rolling force in rolling deformation. Kwak et al. [7] developed an approximate model predicting rolling force and torque applicable to finishing stand of tandem hot strip mill using rigid-viscoplastic FEM. Mori et al. [8] established the formulation of rigid-plastic FEM using diagonal matrix and developed a parallel processing for the large-scale simulation of metal forming processes. The influence of rolling force on the plate shape and final profile was studied by Zhang and Cui [9] using 3D thermo-mechanical coupled elastoplastic FEM. However, FEM is not suitable for on-line control due to large number of computation times and huge memory capacities, so an analytical method is also necessary for actual production.

Narayanasamy [10] used a cosine velocity field to research extrusion and received the upper-bound solution. But, cosine

✉ Yuan-Ming Liu
lymneu@163.com

[1] State Key Laboratory of Rolling and Automation, Northeastern University, Shenyang 110819, Liaoning, People's Republic of China

velocity field has not been reported to be applied to rolling yet. In this paper, a successful method has been presented to compute the analytical solution of rolling force and torque in hot strip finish rolling on the basis of a cosine velocity and strain rate fields which are firstly proposed. The validity of the calculated results is discussed through comparing those with other models' results and on-line measured ones in a hot strip rolling plant.

2 Cosine velocity field

As shown in Fig. 1, the thickness is reduced from $2h_0$ to $2h_1$ (absolute reduction $\Delta h = h_0 - h_1$) while the workpiece is rolled through a pair of cylindrical work rolls with radius of R considering the effect of roll flattening. The horizontal projected length of the roll-workpiece contact arc is given by l, and bite angle is given by θ ($\theta = \sin^{-1}(l/R)$). Cartesian coordinates x, y, and z are defined as length, width, and thickness directions of the workpiece, respectively. The deformation zone of the workpiece is assumed rigid-plastic material [11]. On account of the symmetry of deformation zone, only a quarter is considered, as shown in Fig. 2. The precise equation of contact arc is $h_x = R + h_1 - \sqrt{R^2-(l-x)^2}$, and the first-order derivative equation is $h_x' = -\frac{l-x}{\sqrt{R^2-(l-x)^2}} = -\tan\alpha$.

Note that the shape factor of the workpiece satisfies that the ratio of width/thickness is greater than 10 and $l/(2h_m)>1$ (h_m is the mean half thickness) in finishing zone of hot strip rolling, and then, deformation in the width direction is neglected [4]. The width b can be taken as a constant; hence, $b_0 = b_n = b_1 = b$. Moreover, it is assumed that rolling cross sections remain plane and vertical lines remain straight. Using those assumptions, a new cosine velocity field is proposed:

$$\begin{aligned} v_x &= v_0\left[1+\frac{2}{\pi}\cos\left(\frac{\pi h_x}{2h_0}\right)\right] \\ v_y &= v_0 h_x' y\left\{\frac{1}{h_0}\sin\left(\frac{\pi h_x}{2h_0}\right)-\frac{1}{h_x}\left[1+\frac{2}{\pi}\cos\left(\frac{\pi h_x}{2h_0}\right)\right]\right\} \\ v_z &= \frac{v_0 h_x' z}{h_x}\left[1+\frac{2}{\pi}\cos\left(\frac{\pi h_x}{2h_0}\right)\right] \end{aligned} \quad (1)$$

According to the Cauchy equation, the strain rate components from Eq. (1) are as follows:

$$\begin{aligned} \dot{\varepsilon}_x &= \frac{\partial v_x}{\partial x} = -\frac{v_0 h_x'}{h_0}\sin\left(\frac{\pi h_x}{2h_0}\right) \\ \dot{\varepsilon}_y &= \frac{\partial v_y}{\partial y} = v_0 h_x'\left\{\frac{1}{h_0}\sin\left(\frac{\pi h_x}{2h_0}\right)-\frac{1}{h_x}\left[1+\frac{2}{\pi}\cos\left(\frac{\pi h_x}{2h_0}\right)\right]\right\} \\ \dot{\varepsilon}_z &= \frac{\partial v_z}{\partial z} = \frac{v_0 h_x'}{h_x}\left[1+\frac{2}{\pi}\cos\left(\frac{\pi h_x}{2h_0}\right)\right] \end{aligned} \quad (2)$$

In Eqs. (1) and (2), $\dot{\varepsilon}_x + \dot{\varepsilon}_y + \dot{\varepsilon}_z = 0$; $v_x|_{x=0} = v_0$; $v_y|_{y=0} = 0$; $v_z|_{z=0} = 0$; $v_z|_{z=h_x} = -v_x\tan\alpha$. So, they are kinematically admissible velocity and strain rate fields[12]. The flow volume per second is $U = v_0 h_0 b = v_n h_n b = v_R \cos\alpha_n b(R + h_1 - R\cos\alpha_n)$, where α_n is a neutral angle.

3 EA yield criterion

Equal area (EA) yield criterion is a linear criterion, which covers equal projected area to that of Mises circle on the π-plane. The geometric figure of EA yield criterion on the π-plane is equilateral, but non-equiangular dodecagon intersected with Mises circle locus as shown in Fig. 3.

The formula of the EA yield criterion and the power per unit volume were given by Zhao et al. [13]. The equations of EA yield criterion in the Haigh-Westergaard stress space are as follows ($\sigma_1 > \sigma_2 > \sigma_3$):

$$\begin{aligned} &\sigma_1 - \left(2-\frac{9}{\sqrt{3}\pi}\right)\sigma_2 - \left(\frac{9}{\sqrt{3}\pi}-1\right)\sigma_3 = \sigma_s, \quad \text{if } \sigma_2 \le \frac{1}{2}(\sigma_1+\sigma_3) \\ &\left(\frac{9}{\sqrt{3}\pi}-1\right)\sigma_1 + \left(2-\frac{9}{\sqrt{3}\pi}\right)\sigma_2 - \sigma_3 = \sigma_s, \quad \text{if } \sigma_2 \ge \frac{1}{2}(\sigma_1+\sigma_3) \\ &D(\dot{\varepsilon}_{ij}) = \frac{\sqrt{3}\pi}{9}\sigma_s(\dot{\varepsilon}_{\max} - \dot{\varepsilon}_{\min}) \end{aligned} \quad (3)$$

where σ_s is the material yield stress and $D(\dot{\varepsilon}_{ij})$ is the plastic power per unit volume.

The EA yield criterion had been used in metal rolling [13], calculation of the crack tip plastic zone dimension [14], and so on.

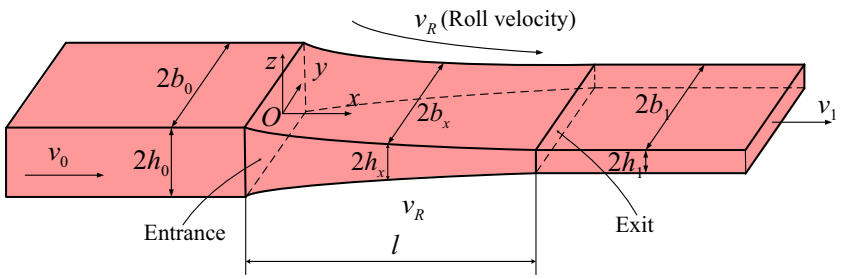

Fig. 1 Deformation of workpiece

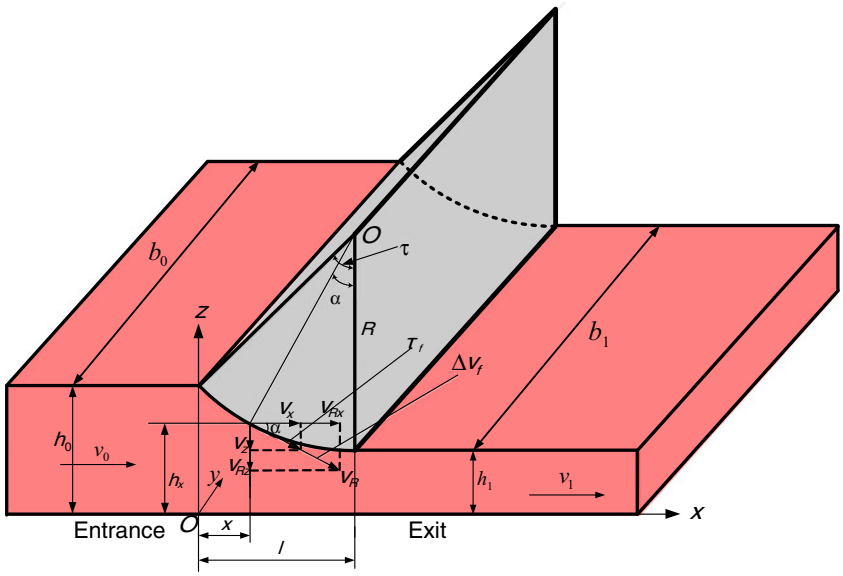

Fig. 2 Definition sketch of the bite zone

4 Total power functional

4.1 Internal plastic deformation power

According to Eq. (2), $\dot{\varepsilon}_{\max} = \dot{\varepsilon}_x$, $\dot{\varepsilon}_{\min} = \dot{\varepsilon}_z$ and substituting these into the Eq. (3), the internal plastic deformation power $\dot{W}_i$ then becomes

$$\begin{aligned}\dot{W}_i &= \int_V D(\dot{\varepsilon}_{ij})\mathrm{d}V = \frac{4\sqrt{3}\pi}{9}\sigma_s\int_0^l\int_0^b\int_0^{h_x}(\dot{\varepsilon}_{\max}-\dot{\varepsilon}_{\min})\mathrm{d}x\mathrm{d}y\mathrm{d}z \\ &= \frac{4\sqrt{3}\pi\sigma_s U}{9}\left\{\varepsilon+\frac{8}{\pi^2}\left[1-\cos\left(\frac{\pi\varepsilon}{2}\right)\right]+\frac{2(1-\varepsilon)}{\pi}\sin\left(\frac{\pi\varepsilon}{2}\right)\right\}\end{aligned} \quad (4)$$

where $\varepsilon = \frac{\Delta h}{h_0}$ is the reduction.

4.2 Friction power

The friction power acts on the interface between the roll and workpiece, as shown in Fig. 2. The roll surface equation is

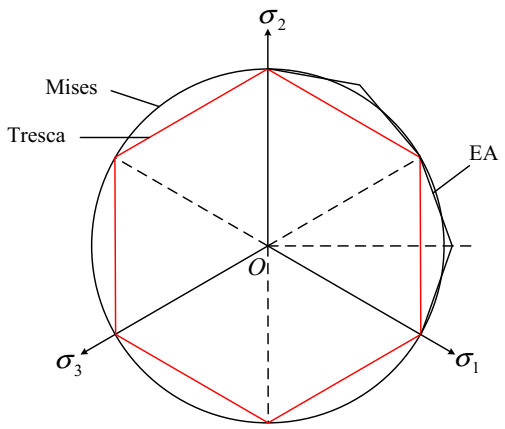

Fig. 3 Locus on the π-plane

$$z = h_x = R + h_1 - \sqrt{R^2-(l-x)^2} \quad (5)$$

The tangential velocity discontinuity $\Delta\boldsymbol{v}_f$ and friction stress $\boldsymbol{\tau}_f = mk$ are always co-linear vector on the interface. The co-line vector inner product [15] is used to integrate the friction power $\dot{W}_f$ as follows:

$$\begin{aligned}\dot{W}_f &= 4\int_0^l\int_0^b \tau_f\left|\Delta v_f\right|\mathrm{d}F = 4\int_0^l\int_0^b \boldsymbol{\tau}_f\Delta\boldsymbol{v}_f\mathrm{d}F \\ &= 4\int_0^l\int_0^b\left(\tau_{fx}\Delta v_x+\tau_{fy}\Delta v_y+\tau_{fz}\Delta v_z\right)\mathrm{d}F \\ &= 4mk\int_0^l\int_0^b\left(\Delta v_x\cos\alpha+\Delta v_y\cos\beta+\Delta v_z\cos\gamma\right)\mathrm{d}F\end{aligned} \quad (6)$$

where $k = \sigma_s/\sqrt{3}$ is the yield shear stress, α, β, γ are the angles between $\Delta\boldsymbol{v}_f$ and the directions of x, y, and z axes, respectively. Differential element area of the roll surface from Eq. (5) is $\mathrm{d}F = \sqrt{1+\left(h_x'\right)^2}\mathrm{d}x\mathrm{d}y = \sec\alpha\mathrm{d}x\mathrm{d}y$. And then, the values of direction cosines are as follows

$$\cos\alpha = \pm\frac{\sqrt{R^2-(l-x)^2}}{R} \quad \cos\gamma = \pm\frac{(l-x)}{R} = \sin\alpha \quad \cos\beta = 0 \quad (7)$$

The components of tangential velocity discontinuity $\Delta\boldsymbol{v}_f$ along roll surface from Eq. (1) are respectively:

$$\begin{aligned}\Delta v_x &= v_R\cos\alpha - v_0\left[1+\frac{2}{\pi}\cos\left(\frac{\pi h_x}{2h_0}\right)\right] \\ \Delta v_y &= -v_0 h_x' y\left\{\frac{1}{h_0}\sin\left(\frac{\pi h_x}{2h_0}\right)-\frac{1}{h_x}\left[1+\frac{2}{\pi}\cos\left(\frac{\pi h_x}{2h_0}\right)\right]\right\} \\ \Delta v_z|_{z=h_x} &= v_R\sin\alpha - v_0\tan\alpha\left[1+\frac{2}{\pi}\cos\left(\frac{\pi h_x}{2h_0}\right)\right]\end{aligned} \quad (8)$$

Substituting Eqs. (7) and (8) into Eq. (6) and integrating, then obtains

$$W_f = 4mkb\left\langle \int_0^l \left\{ v_R\cos\alpha - v_0\left[1+\frac{2}{\pi}\cos\left(\frac{\pi h_x}{2h_0}\right)\right]\right\}\mathrm{d}x + \int_0^l \left\{ v_R\sin\alpha - v_0\tan\alpha\left[1+\frac{2}{\pi}\cos\left(\frac{\pi h_x}{2h_0}\right)\right]\right\}\tan\alpha\,\mathrm{d}x\right\rangle = 4mkb\left(I_{f1}+I_{f2}\right) \tag{9}$$

$$I_{f1} = \int_0^{x_n}\left\{ v_R\cos\alpha - v_0\left[1+\frac{2}{\pi}\cos\left(\frac{\pi h_x}{2h_0}\right)\right]\right\}\mathrm{d}x - \int_{x_n}^{l}\left\{ v_R\cos\alpha - v_0\left[1+\frac{2}{\pi}\cos\left(\frac{\pi h_x}{2h_0}\right)\right]\right\}\mathrm{d}x = v_R R\left(\frac{\theta}{2}-\alpha_n+\frac{\sin 2\theta}{4}-\frac{\sin 2\alpha_n}{2}\right) + \mathrm{g}_f v_0 R\sin\alpha_n + \mathrm{g}_b v_0 R(\sin\alpha_n - \sin\theta) \tag{10}$$

$$I_{f2} = \int_0^{x_n}\left\{ v_R\sin\alpha\tan\alpha - v_0\tan^2\alpha\left[1+\frac{2}{\pi}\cos\left(\frac{\pi h_x}{2h_0}\right)\right]\right\}\mathrm{d}x - \int_{x_n}^{l}\left\{ v_R\sin\alpha\tan\alpha - v_0\tan^2\alpha\left[1+\frac{2}{\pi}\cos\left(\frac{\pi h_x}{2h_0}\right)\right]\right\}\mathrm{d}x = v_R R\left(\frac{\theta}{2}-\alpha_n+\frac{\sin 2\alpha_n}{2}-\frac{\sin 2\theta}{4}\right) + \mathrm{g}_b v_0 R\left[\ln\frac{\tan\left(\pi/4+\alpha_n/2\right)}{\tan\left(\pi/4+\theta/2\right)} + \sin\theta - \sin\alpha_n\right] + \mathrm{g}_f v_0 R\left[\ln\tan\left(\pi/4+\alpha_n/2\right) - \sin\alpha_n\right] \tag{11}$$

where g_b and g_f are the parameters, $\mathrm{g}_b = 1+\frac{2}{\pi}\cos\left(\frac{\pi h_{mb}}{2h_0}\right)$ and $\mathrm{g}_f = 1+\frac{2}{\pi}\cos\left(\frac{\pi h_{mf}}{2h_0}\right)$. Mean thickness of workpiece between entry and neutral plane is $h_{mb} = \frac{h_0+h_{\alpha_n}}{2}$,, and mean thickness of workpiece between exit and neutral plane is $h_{mf} = \frac{h_1+h_{\alpha_n}}{2}$.

Substituting Eqs. (10) and (11) into Eq. (9), then gives

$$\dot{W}_f = 4mkbR\left[v_R(\theta-2\alpha_n) + \frac{U}{h_0 b}\left(\mathrm{g}_b\ln\frac{\tan\left(\pi/4+\alpha_n/2\right)}{\tan\left(\pi/4+\theta/2\right)} + \mathrm{g}_f\ln\tan\left(\pi/4+\alpha_n/2\right)\right)\right] \tag{12}$$

4.3 Shear power

In the exit section ($x=l$) of deformation zone according to Eq. (1), there is $h'_{x=l}=h'_{\alpha=0}=0$, $\nu_z|_{x=l}=\nu_y|_{x=l}=0$. Therefore, there is no shear power in the exit section. But, on the entry section ($x=0$)

$$v_y|_{x=0} = 0, \quad v_z|_{x=0} = -\frac{v_0\tan\theta}{h_0}z \tag{13}$$

Then, the shear power $\dot{W}_s$ is [16]

$$\dot{W}_s = 4k\int_0^{h_0}\int_0^{b_0}|\Delta v_t|\mathrm{d}y\mathrm{d}z = 4k\int_0^{h_0}\int_0^{b_0}\sqrt{v_y^2+v_z^2}\mathrm{d}y\mathrm{d}z = 4k\int_0^{b}\int_0^{h_0}\frac{v_0\tan\theta}{h_0}z\mathrm{d}y\mathrm{d}z = 2kbh_0v_0\tan\theta = 2kU\tan\theta \tag{14}$$

4.4 Total deformation power and its minimization

Substituting Eqs. (4), (12), and (14) into $\Phi = \dot{W}_i + \dot{W}_f + \dot{W}_s$, an analytical solution of total deformation power functional Φ is

$$\Phi = \frac{4\sqrt{3}\pi\sigma_s U}{9}\left\{\varepsilon + \frac{8}{\pi^2}\left[1-\cos\left(\frac{\pi\varepsilon}{2}\right)\right] + \frac{2(1-\varepsilon)}{\pi}\sin\left(\frac{\pi\varepsilon}{2}\right)\right\} + 2kU\tan\theta + 4mkbR\left[v_R(\theta-2\alpha_n) + \frac{U}{h_0 b}\left(\mathrm{g}_b\ln\frac{\tan\left(\pi/4+\alpha_n/2\right)}{\tan\left(\pi/4+\theta/2\right)} + \mathrm{g}_f\ln\tan\left(\pi/4+\alpha_n/2\right)\right)\right] \tag{15}$$

The total power of Eq. (15) is minimized with respect to the arbitrary variable α_n, and then, the value

closest to the actual power required is got. The following equation can be obtained

$$\frac{\mathrm{d}\Phi}{\mathrm{d}\alpha_n}=\frac{\mathrm{d}\dot{W}_i}{\mathrm{d}\alpha_n}+\frac{\mathrm{d}\dot{W}_s}{\mathrm{d}\alpha_n}+\frac{\mathrm{d}\dot{W}_f}{\mathrm{d}\alpha_n}=0 \tag{16}$$

where

$$\frac{\mathrm{d}\dot{W}_i}{\mathrm{d}\alpha_n}=\frac{4\sqrt{3}\pi\sigma_s N}{9}\left\{\varepsilon+\frac{8}{\pi^2}\left[1-\cos\left(\frac{\pi\varepsilon}{2}\right)\right]+\frac{2(1-\varepsilon)}{\pi}\sin\left(\frac{\pi\varepsilon}{2}\right)\right\} \tag{17}$$

$$\frac{\mathrm{d}\dot{W}_f}{\mathrm{d}\alpha_n}=4mkbR\left\{-2v_R+\frac{N}{h_0 b}\left[\mathrm{g}_b\ln\frac{\tan\left(\pi/4+\alpha_n/2\right)}{\tan\left(\pi/4+\theta/2\right)}+\mathrm{g}_f\ln\tan\left(\pi/4+\alpha_n/2\right)\right]+\frac{U\left(\mathrm{g}_b+\mathrm{g}_f\right)}{h_0 b\cos\alpha_n}-\frac{UR\sin\alpha_n}{2h_0^2 b}\left[\sin\left(\frac{\pi h_{mb}}{2h_0}\right)\ln\frac{\tan\left(\pi/4+\alpha_n/2\right)}{\tan\left(\pi/4+\theta/2\right)}+\sin\left(\frac{\pi h_{mf}}{2h_0}\right)\ln\tan\left(\pi/4+\alpha_n/2\right)\right]\right\} \tag{18}$$

$$\frac{\mathrm{d}\dot{W}_s}{\mathrm{d}\alpha_n}=2kN\tan\theta \tag{19}$$

where $N=\frac{\mathrm{d}U}{\mathrm{d}\alpha_n}=v_R bR\sin 2\alpha_n - {}_v Rb(R+h_1)\sin\alpha_n$. The friction factor can be deduced as follows:

$$m=\frac{\frac{\sqrt{3}\pi\sigma_s N}{9}\left\{\varepsilon+\frac{8}{\pi^2}\left[1-\cos\left(\frac{\pi\varepsilon}{2}\right)\right]+\frac{2(1-\varepsilon)}{\pi}\sin\left(\frac{\pi\varepsilon}{2}\right)\right\}+\frac{kN\tan\theta}{2}}{kbR\left\{2v_R-\frac{N}{h_0 b}\left[\mathrm{g}_b\ln\frac{\tan\left(\pi/4+\alpha_n/2\right)}{\tan\left(\pi/4+\theta/2\right)}+\mathrm{g}_f\ln\tan\left(\pi/4+\alpha_n/2\right)\right]-\frac{U\left(\mathrm{g}_b+\mathrm{g}_f\right)}{h_0 b\cos\alpha_n}+\frac{UR\sin\alpha_n}{2h_0^2 b}\left[\sin\left(\frac{\pi h_{mb}}{2h_0}\right)\ln\frac{\tan\left(\pi/4+\alpha_n/2\right)}{\tan\left(\pi/4+\theta/2\right)}+\sin\left(\frac{\pi h_{mf}}{2h_0}\right)\ln\tan\left(\pi/4+\alpha_n/2\right)\right]\right\}} \tag{20}$$

The optimal values of α_n in various production conditions are obtained by solving Eq. (16). The minimum of total power $\Phi_{\min}$ can be obtained by substituting α_n into Eq. (15) [17]. Then, the corresponding minimum values of rolling torque $M_{\min}$, rolling force $F_{\min}$, and stress effective factor n_σ (χ is the arm factor) can be determined, respectively [18]:

$$M_{\min}=\frac{R\Phi_{\min}}{2v_R}\quad F_{\min}=\frac{M_{\min}}{\chi\cdot\sqrt{2R\Delta h}}\quad n_\sigma=\frac{F_{\min}}{4bl\,k} \tag{21}$$

Considering the effect of roll flattening on the rolling force, the roll flattening model used in calculation is determined by Sun [19]

$$R=R_0\left(1+2.2\times10^{-5}\frac{F_{\min}}{b\Delta h}\right) \tag{22}$$

where R_0 is the original radius of work roll. The computing flow chart is shown in Fig. 4, and the process ends when the radius is convergent. The condition of convergence is $\frac{|R_i-R_{i-1}|}{R_i}\le 0.01$ in this paper.

5 Calculation and discussion

Practical data of rolling force measured in a factory are used to verify the analytical result calculated in this paper. Taking the material of Q235B steel product, for example, the workpiece thickness is reduced from 50 to 5.7 mm in the seven finishing stands; the width is 510 mm. Table 1 gives the roll circumferential velocity v_R and temperature t of no. 1 to no. 7 stands in finishing mill. The regression model of deformation resistance for the Q235B steel used in the calculation is determined by the formula in Ref. [19], and it can be expressed as follows:

$$\sigma_s=\sigma_0 e^{(a_1T+a_2)}\left(\frac{\dot{E}}{10}\right)^{(a_3T+a_4)}\left[a_6\left(\frac{E}{0.4}\right)^{a_5}-(a_6-1)\frac{E}{0.4}\right] \tag{23}$$

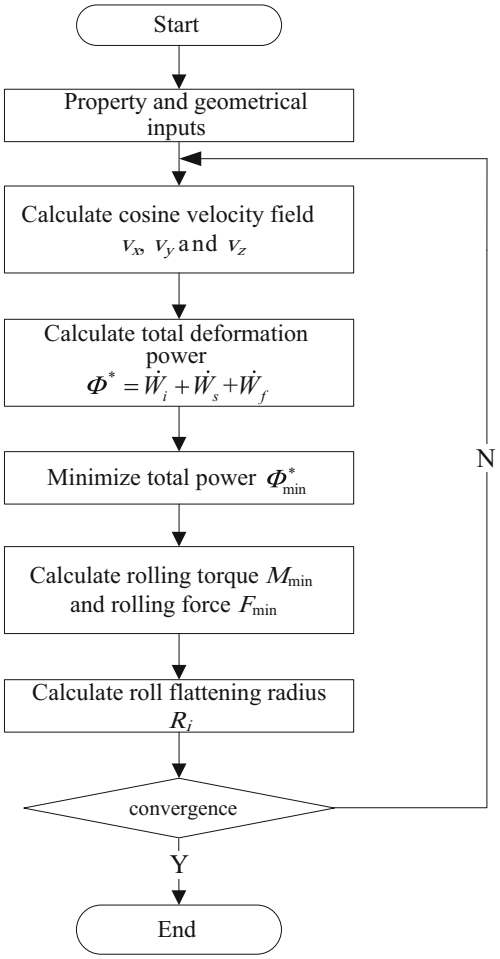

Fig. 4 Flow chart of the calculation

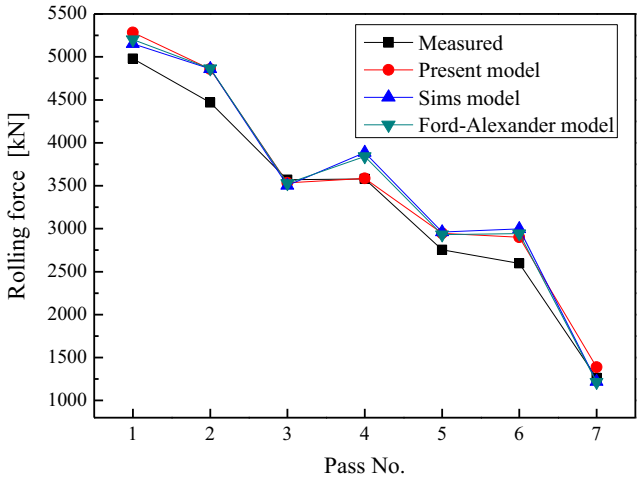

Fig. 5 Comparison rolling force predicted by present model with other researchers' and measured results

where σ_0=139.8MPa, a_1=−2.861, a_2=3.642, a_3=0.254, a_4=−0.1993, a_5=0.4349, a_6=1.51, $T = \frac{t+273}{1000}$, and t is the deformation temperature. Equation (23) shows that deformation resistance is a function of rolling temperature t, true strain E, and strain rate Ė

The rolling forces of analytical result are calculated by Eq. (21) and then compared with measured ones and the analytical results of Sims [20] and Ford-Alexander [21] ones as shown in Fig. 5.

According to Fig. 5, due to the nature of the upper-bound method, the calculated rolling forces are slightly higher than the measured ones. However, the errors are less than 9.51 %. The results of the present model are in a good agreement with Sims and Ford-Alexander ones within 8.5 % error. The model of deformation resistance is chosen from the reference which was regressed the data from laboratory experiment. The comparison errors may be made large by this model. The model of deformation resistance may be regressed from the data in the actual production, which is to be left as a future work. Results show that the proposed cosine velocity field is reliable and adequate enough to be applied in the process control of hot strip finish rolling.

Figure 6 illustrates that the rolling torque and force increase linearly with the increasing of reduction ε. While Δh increases, the length of deformation zone and the volume of compressed metal increase, and then, the rolling force increases subsequently.

Figure 7 shows that the shear power $\dot{W}_s$ is smaller than the internal plastic deformation power $\dot{W}_i$ and friction power $\dot{W}_f$. Since the workpiece used in the present paper is thin, then friction power increases with the increasing of reduction ε.

It can be seen from Fig. 8 that the location of neutral point x_n/l is affected by the reduction ε and friction factor m. When ε increases or m decreases, the neutral point moves toward the exit plane. Besides, the neutral

Table 1 Rolling conditions in a factory

Pass No.	1	2	3	4	5	6	7
v_R (m s^{-1})	0.94	1.32	1.9	2.8	3.8	5.12	6.02
t (°C)	1040.94	1032.23	1023.37	1015.41	1008.03	998.44	992.67
E=ln(h_0/h_1)	0.352	0.343	0.357	0.394	0.294	0.293	0.125
σ_s (MPa)	108.58	119.07	136.94	153.43	155.14	167.42	130.66

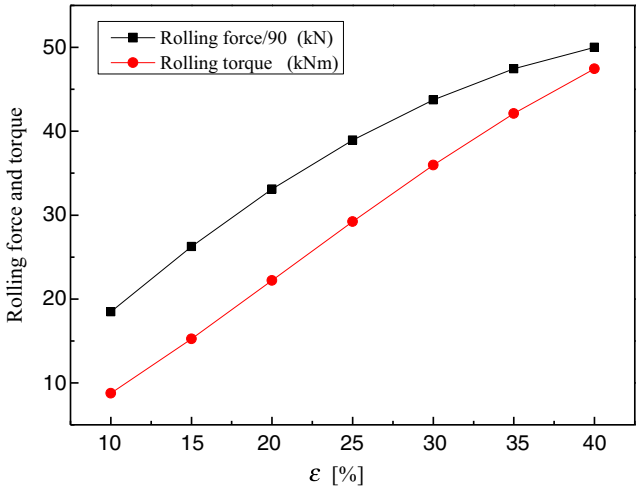

Fig. 6 Rolling force and torque with different reduction ε

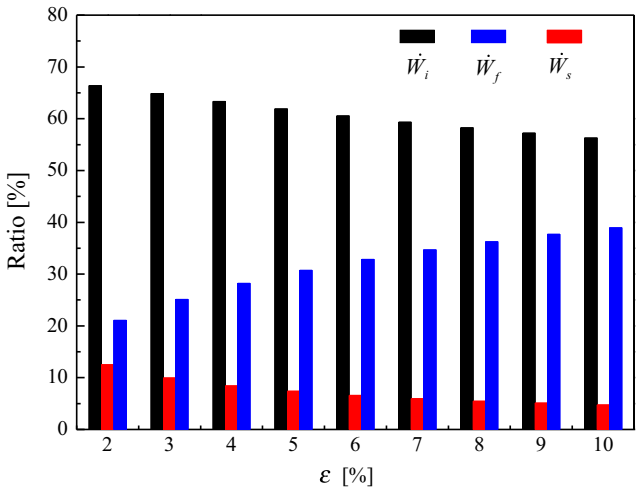

Fig. 7 Ratio of $\dot{W}_i$, $\dot{W}_f$, and $\dot{W}_s$ to $\Phi_{\min}$ with different reduction ε

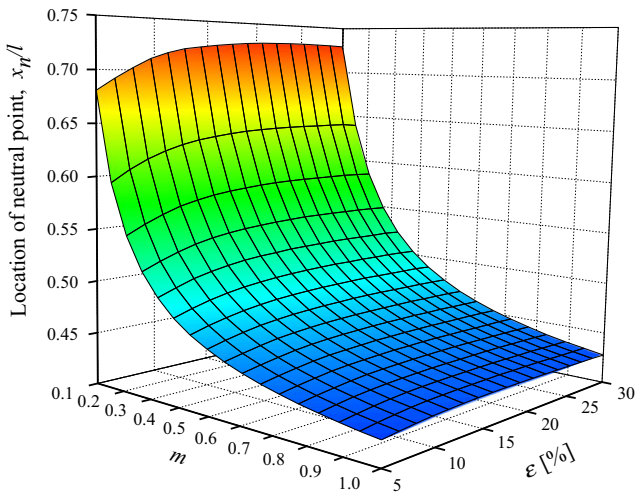

Fig. 8 Effect of m and ε on location of neutral points

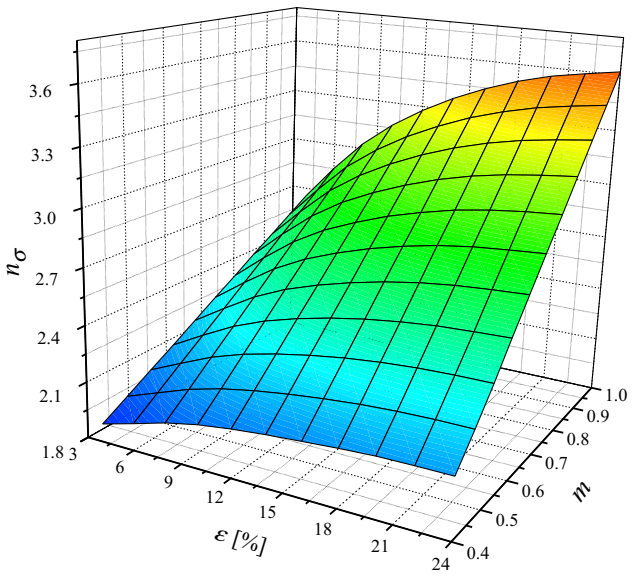

Fig. 9 Effect of ε and m on n_σ

point location changes obviously with a small change in friction for $m<0.3$.

It can be seen from Fig. 9 that the reduction ε and friction factor m influence the stress state coefficient n_σ obviously. And, the n_σ increases with the increasing of ε or m. In addition, the effect of m on the n_σ is obvious, which is consistent with the result shown in Fig. 7.

Figure 10 displays the effect of deformation factors $l/(2h_m)$ and R/h_0 on stress state coefficient n_σ. It can be seen that n_σ increases as $l/(2h_m)$ or R/h_0 increases.

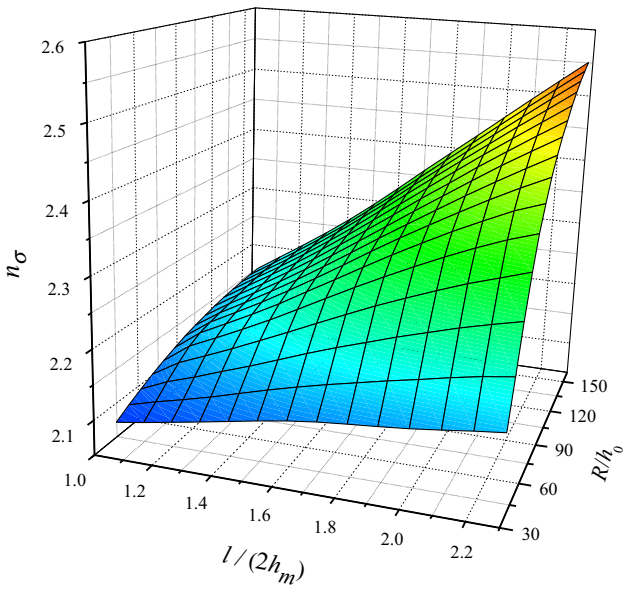

Fig. 10 Effect $l/(2h_m)$ of and R/h_0 on n_σ

6 Conclusions

1. The cosine velocity field satisfying kinematically admissible condition is firstly proposed to be applied in hot strip finish rolling process. The analytical solutions of rolling torque, rolling force, and stress effective factor are obtained using the field and EA yield criterion.
2. The error of calculated required optimum rolling forces is within 9.51 % compared with measured ones and less than 8.5 % compared with Sims and Ford-Alexander's results. The analytical solutions are reliable and adequate enough to research finish rolling process.
3. While friction factor m decreases or reduction ε increases, the neutral point moves toward the exit. Both rolling force and torque increase with the increasing of reduction ε.
4. The stress factor n_σ increases while the shape factor $l/(2h_m)$, ε, R/h_0, or friction factor m increases.

Acknowledgments This study is financially supported by the National Natural Science Foundation of China (No.: 51074052, 50734002), the Fundamental Research Funds for the Central Universities (No.: N140704001), and the PhD Start-up Fund of Natural Science Foundation of Liaoning Province, China (No.: 20131033).

References

1. Hill R (1963) A general method of analysis for metal-working processes. J Mech Phys Solids 11(5):305–326
2. Oh SI, Kobayashi S (1975) An approximate method for a three-dimensional analysis of rolling. Int J Mech Sci 17(4):293–305
3. Martins PAF, Marques MJMB (1999) Upper bound analysis of plane strain rolling using a flow function and the weighted residuals method. Int J Numer Meth Eng 44(11):1671–1683. doi:10.1002/(Sici)1097-0207(19990420)44:11<1671::Aid-Nme559>3.0.Co;2-2
4. Sezek S, Aksakal B, Can Y (2008) Analysis of cold and hot plate rolling using dual stream functions. Mater Design 29(3):584–596. doi:10.1016/j.matdes.2007.03.005
5. Kobayashi S, Oh SI, Altan T (1989) Metal forming and the finite-element method. Oxford university press, New York
6. Mori K, Osakada K (1990) Finite element simulation of three-dimensional deformation in shape rolling. Int J Numer Meth Eng 30(8):1431–1440
7. Kwak WJ, Kim YH, Park HD, Lee JH, Hwang SM (2000) FE-based on-line model for the prediction of roll force and roll power in hot strip rolling. ISIJ Int 40(10):1013–1018. doi:10.2355/isijinternational.40.1013
8. Mori K, Otomo Y, Yoshimura H (2006) Parallel processing of 3D rigid-plastic finite element method using diagonal matrix. J Mater Process Technol 177(1–3):63–67. doi:10.1016/j.jmatprotec.2006.04.064
9. Zhang JL, Cui ZS (2011) Continuous FEM simulation of multi-pass plate hot rolling suitable for plate shape analysis. J Cent South Univ T 18(1):16–22. doi:10.1007/s11771-011-0652-3
10. Narayanasmy R, Ponalagusamy R, Venkatesan R, Srinivasan P (2006) An upper bound solution to extrusion of circular billet to circular shape through cosine dies. Mater Design 27(5):411–415. doi:10.1016/j.matdes.2004.11.026
11. Chandra S, Dixit US (2004) A rigid-plastic finite element analysis of temper rolling process. J Mater Process Technol 152(1):9–16. doi:10.1016/j.jmatprotec.2003.11.003
12. Tabatabaei SA, Abrinia K, Givi MKB (2014) Application of equi-potential lines method for accurate definition of the deforming zone in the upper-bound analysis of forward extrusion problems. Int J Adv Manuf Tech 72(5–8):1039–1050. doi:10.1007/s00170-014-5647-4
13. Zhao DW, Fang Q, Li CM, Liu XH, Wang GD (2010) Derivation of plastic specific work rate for equal area yield criterion and its application to rolling. J Iron Steel Res Int 17(4):34–38
14. Lan LY, Li CM, Zhao DW, Qiu CL (2012) Derivation of equal area criterion and its application to crack tip plastic zone analysis. Appl Mech Mat 110:2918–2925
15. Liu YM, Zhang DH, Zhao DW, Sun J (2015) Analysis of vertical rolling using double parabolic model and stream function velocity field. Int J Adv Manuf Tech. doi:10.1007/s00170-015-7393-7
16. Abrinia K, Mirnia MJ (2009) A new generalized upper-bound solution for the ECAE process. Int J Adv Manuf Tech 46(1–4):411–421. doi:10.1007/s00170-009-2103-y
17. Hua L, Deng JD, Qian DS, Ma Q (2014) Using upper bound solution to analyze force parameters of three-roll cross rolling of rings with small hole and deep groove. Int J Adv Manuf Tech 76(1–4):353–366. doi:10.1007/s00170-014-6107-x
18. Zhang SH, Zhao DW, Gao CR (2012) The calculation of roll torque and roll separating force for broadside rolling by stream function method. Int J Mech Sci 57(1):74–78. doi:10.1016/j.ijmecsci.2012.02.006
19. Sun YK (2010) Model and control of cold and hot rolling mill for sheets and strips. Metallurgical Industry Press, Beijing
20. Sims RB (1954) The calculation of roll force and torque in hot rolling mills. Proc I Mech Eng 168(1954):191–200. doi:10.1243/pime_proc_1954_168_023_02
21. Gupta S, Ford H (1967) Calculation method for hot rolling of steel sheet and strip. J Iron Steel Institute 205(2):186–190